2

Method and model

A detailed knowledge of catalysis and surface chemistry at a molecular level is crucial to understanding chemical processes. Theoretical simulations can provide a better interpretation of experimental results and provide information that cannot be obtained or is difficult to obtain experimentally. The last few years have seen enormous improvements in computer capacity and speed. There is now a wide and increasing variety of methods in Computational Chemistry. We are able to perform electronic structure calculations on models of sufficient size to represent the 'chemistry' occurring at surfaces. Computational Chemistry tools can reliably predict interaction energies, geometric structures and electronic properties.

This chapter is organised as follows: section 2.1 introduces the Born-Oppenheimer approximation; section 2.2 summarises the basic principles of Density Functional Theory; section 2.3 describes the common strategies for dealing with infinite systems; section 2.4 briefly explains pseudopotential approximation; section 2.5 summarises the key features of the program used to perform the calculations, VASP; section 2.6 discusses the fundamental principles of RAIRS and HREELS spectroscopies and develops the approximations used in this thesis to simulate the vibrational spectra; section 2.7 describes the transition state search algorithms currently available in VASP and the strategies used in this thesis to find saddle points; section 2.8 discusses the calculation of the Density of States; section 2.9 summarises the approximations used to construct the pressure and temperature phase diagrams and section 2.10 presents and discusses some computational details of this thesis.

2.1 Born-Oppenheimer approximation

The *Schrödinger equation* is the key equation of the science of quantum mechanics. This equation, developed by the physicist Erwin Schrödinger in 1925-26, has the same central importance to quantum mechanics as Newton's laws of motion have to the large-scale phenomena of classical mechanics.

For a system composed of *N* electrons and *M* nuclei, it is expressed as:

$$\hat{H}\Psi_n\left(\{\vec{r}_i\}\{\vec{R}_\mu\}\right) = E_n\Psi_n\left(\{\vec{r}_i\}\{\vec{R}_\mu\}\right) \tag{2.1}$$

where $\hat{H}$ is the time-independent Hamiltonian, Ψ_n is the wave function of the system associated to the energy level E_n (*n* accounts for the quantisation of the system) and $\vec{r}_i$ and $\vec{R}_\mu$ are the spatial coordinates of the electrons and the nuclei, respectively. All the properties of the electron-nuclei system are described by **equation 2.1** (except for relativistic effects). By solving this equation we therefore obtain all the physico-chemical properties of the target system. Unfortunately, this involves dealing with a system of *(N+M)* interacting particles. Even for a very small system, this process is too complex to solve (even numerically!). To solve the Schrödinger equation, therefore, several approximations are needed.

For systems with many variables, a common way to simplify complicated equations is to separate the variables. One such separation step, universally accepted in electronic structure theory, is the separation of nuclear and electronic motion—the so-called *Born-Oppenheimer approximation* [1]. This approximation is based on the difference in mass between nuclei and electrons. The lightest nucleus, the one of the hydrogen atom, is actually 1,836 times heavier than an electron. We can therefore consider nuclear and electronic motion as independent. Electrons follow nuclei instantaneously during the motion of the latter, i.e. they change their wave function very quickly with respect to the timescale of nuclei. We can then rewrite the expression for the Hamiltonian as

$$\hat{H} = \hat{T}_{nuc} + \hat{H}_{el} \tag{2.2}$$

The electronic Hamiltonian $\hat{H}_{el}$ depends parametrically on nuclear positions (R_{μ}): the nuclear coordinates appear in the electronic Hamiltonian, but derivatives with respect to these coordinates do not. Therefore, the electronic problem can be solved for nuclei that are momentarily fixed in space.

$$\hat{H}_{el}(r,R)\psi_{el}(r,R) = E_{el}(R)\psi_{el}(r,R) \tag{2.3}$$

R and r are the total set of nuclear and electronic coordinates. The total wave function can then be approximated as a product

$$\Psi_{BO}(r,R) = \psi_{nuc}(R)\psi_{el}(r,R) \tag{2.4}$$

where the nuclear wave function $\psi_{nuc}(R)$ is a solution to the equation

$$\{\hat{T}_{nuc}(R) + E_{el}(R)\}\psi_{nuc}(R) = E\psi_{nuc}(R) \tag{2.5}$$

Separation of the electronic and nuclear wave functions clearly simplifies the resolution of the Schrödinger equation. The determination of the total wave function of the system nuclei plus electrons is reduced to the determination of the total electronic wave function. However, for systems with hundreds or even thousands of electrons the electronic part of the problem is too complicated to be treated exactly.

First-principle quantum chemical methods are intended to solve *ab initio* ('from scratch') the electronic Schrödinger equation. *Ab initio* methods include wave function methods—e.g. Hartree-Fock (HF), Configuration Interaction (CI) theory, Perturbation theory (PT) and coupled Cluster Methods (CC)—and Density Functional Theory (DFT) methods [2–7]. The former, which can provide extremely accurate results if a high level of Configuration Interactions is included, are limited to 10–100 electrons because of the great scaling with the system size. For transition metal surfaces its application is therefore restricted to quite small systems (tens of atoms). This usually makes these methods

unattractive to model transition metal catalysts. In fact, in surface science and catalysis they are mainly used as benchmarks [8] that can be used to gauge the accuracy of less computational-time-demanding DFT methods. Density Functional Theory has therefore been used for the calculations in this thesis. In the next section we briefly report the bases of this method.

2.2 Density Functional Theory

In the mid 1920s, Thomas and Fermi [9] made a crucial advance towards the resolution of the electronic Hamiltonian. They established that the energy of a homogeneous electron gas is a function of its electronic density. In 1964, Hohenberg and Kohn [10] showed that this principle can be generalised to any kind of electronic system and established the basis of *Density Functional Theory* (DFT). For a system of N electrons and M nuclei, the electronic Hamiltonian can be written as

$$\hat{H} = \hat{T} + \hat{V} + \hat{W} \tag{2.6}$$

The first term in equation (**2.6**), $\hat{T}$, is the kinetic energy arising from the motion of electrons, the second term is the potential energy of the nuclear-electron attraction, $\hat{V}$, and the third term is the electron-electron repulsion, $\hat{W}$.

Hohenberg and Kohn proved that the ground-state molecular energy, wave function, and all other molecular properties are uniquely determined by the exact electron density, $\rho(\vec{r})$. Therefore, the central focus of DFT is the electronic density, ρ, rather than the wave function, ψ. If N is the number of electrons, the density function, $\rho(\vec{r})$, is defined by

$$\rho(r) = N \int ... \int |\psi|^2 ds_1 dr_2 ... dr_N \tag{2.7}$$

where ψ is the electronic wave function of the system. Then

$$\int \rho(r)dr = N \tag{2.8}$$

DFT is based on two main theorems, the first and second *Hohenberg-Kohn theorems:*
Theorem 1. *The external potential $\hat{V}$ is a unique functional of ρ; since V fixes the Hamiltonian, the particle ground state is a unique functional of ρ. Therefore, there is a direct relationship between the electronic density and the energy (and its individual parts).*

$$E[\rho] = T[\rho] + V[\rho] + W[\rho] \tag{2.9}$$
$$V[\rho] = \int \rho(r)v(r)dr \tag{2.10}$$

Theorem 2. *For a trial density* $\rho(\vec{r})$, *such as* $\rho(\vec{r}) \geq 0$ *and* $\int \rho(r) dr = N$, $E_0[\rho_0] \leq E[\rho]$. *In other words, the energy of the system* $E[\rho]$ *reaches a minimum value* E_0 *for the exact density* ρ_0. *This is the so-called variational principle.*

If we take a closer look at equation (**2.9**), we can separate the $W[\rho]$ functional into two contributions: the classic interaction between two charge densities (Coulomb) and a second term that contains the non-classical parts (**eq. 2.11**).

$$W[\rho] = \frac{1}{2} \iint \frac{\rho(\vec{r}_1)\rho(\vec{r}_2)}{r_{12}} d\vec{r}_1 d\vec{r}_2 + W_{NCL}[\rho] = W_{CL}[\rho] + W_{NCL}[\rho] \qquad (2.11)$$

The complete energy functional can be expressed as

$$E[\rho] = T[\rho] + V[\rho] + W_{CL}[\rho] + W_{NCL}[\rho] \qquad (2.12)$$

In equation (**2.12**) only the $V[\rho]$ and $W_{CL}[\rho]$ terms are known. To solve the problem of the kinetic energy functional, this term is split into two contributions: $T_s[\rho]$ and $T_c[\rho]$. The former is expressed as a one-particle approach (**2.13**) and the latter, still unknown, contains the difference between the real functional and the one particle term.

$$T_s[\rho] = \frac{1}{2} \sum_i \langle \psi_i | \nabla^2 | \psi_i \rangle \qquad (2.13)$$

Equation (**2.12**) can be rewritten as follows

$$E[\rho] = T_s[\rho] + T_c[\rho] + V[\rho] + W_{CL}[\rho] + W_{NCL}[\rho] \qquad (2.15)$$
$$= T_s[\rho] + V[\rho] + W_{CL}[\rho] + E_{XC}[\rho]$$

where the $E_{XC}[\rho]$ or *exchange-correlation functional* contains all the unknown terms (all the many-body interactions).

Unfortunately, the Hohenberg and Kohn theorems do not tell us how to calculate E_0 from ρ since the exact form of the functional is not known. Kohn and Sham [11] invented an indirect approach to this functional. In the *Kohn-Sham method*, the exact ground state can be found from the Kohn-Sham orbitals,

$$\rho(r) = \sum_i |\psi_i(r)|^2 \qquad (2.16)$$

The Kohn-Sham orbitals are obtained from the one-electron Kohn-Sham equations

$$f_s^{KS}\psi_i = \varepsilon_i\psi_i \tag{2.17}$$

where f_s^{KS} is

$$f_s^{KS} = -\frac{1}{2}\nabla^2 - \int \frac{\rho(\vec{r}_2)}{r_{12}}d\vec{r}_2 + \sum_\mu \frac{Z_\mu}{r_{1\mu}} + \nu(r) \tag{2.18}$$

These equations are solved iteratively. Thus, we propose a guess density, which is used to build the f_s^{KS}, then we solve the set of equations (**2.17**) and obtain a new density, which is used to build a second f_s^{KS}, until self-consistency is reached. No one knows what the exact functional $E_{XC}[\rho]$ is. Finding the analytical expression of the exchange-correlation term is a major task in DFT. Some approximate functionals have been proposed.

2.2.1 The exchange-correlation functional

To describe $E_{XC}[\rho(r)]$, two approximations are generally used: the *Local Density Approximation* (LDA) and the *Generalised Gradient Approximation* (GGA).

LDA is based on a model called uniform electron gas [9]. This approximation assumes that the charge density varies slowly throughout a molecule so that a localised region of the molecule behaves like a uniform electron gas. The exchange-correlation energy is then expressed as a function of the exchange-correlation functional per particle of a uniform electron gas, ε_{XC}.

$$E_{XC}^{LDA}[\rho(r)] = \int \rho(r)\varepsilon_{XC}[\rho(r)]dr \tag{2.19}$$

The energy functional accounts for the local value of ρ at each point in space regardless of any other point. Vosko, Wilk and Nusair (VWN) [12] reported the first analytic expression for the correlation term within this approximation.

GGA adds an additional term to the LDA exchange-correlation energy. Gradient corrections are introduced to allow exchange-correlation functional to vary (the density gradient is taken into account). $E_{XC}[\rho(r)]$ is expressed as

$$E_{XC}^{GGA}[\rho(r)] = \int f_{XC}(\rho(r),|\nabla\rho(r)|)\rho(r)dr \tag{2.20}$$

There are many exchange-correlation expressions in the literature, e.g. Perdew (P86), Becke (B86, B88), Perdew-Wang (PW91), Laming-Termath-Handy (CAM) and Perdew-Burke-Enzerhof (PBE) for the exchange part and Perdew (P86), Lee-Yang-Parr (LYP), Perdew-Wang (PW91) and Perdew-Burke-Enzerhof (PBE) for the correlation term [13].

There is a third class of functionals in DFT called *hybrid functionals*, like the popular B3LYP [14] exchange-correlation functional. These include the exact exchange energy as a contribution from the exact exchange. This approach has extensively proven its accuracy for many systems, although they are more time-demanding than *non-hybrid* exchange-correlation functionals because of the calculation of the two-electron integrals in the exact exchange.

We chose the PW91 exchange-correlation functional for all the calculations performed in this thesis because of its good description of the chemical bond [15].

If the exact form of E_{xc} is unknown, one cannot say very much about the performance of a new functional until it is tested with different chemical systems. The exchange-correlation functional is still the most restrictive approximation in DFT calculations. Unfortunately, other approximations are needed to cope with the systems studied in this thesis (hydrocarbons on transition metal surfaces).

2.3 Periodic calculations

Metal crystals have an infinite number of atoms. Working with a system with an infinite number of atoms implies that the wave function has to be calculated for each of the infinite number of electrons and the basis set in which the wave function is expressed will be also infinite. In this section we briefly describe how to overcome these difficulties.

2.3.1 Modelling a periodic system

We are essentially interested in metallic surfaces. These bi-dimensional systems can be modelled by two different approaches: the finite, or the so-called *cluster model approach* [16–19], and the *periodic* or *slab model* [17,20]. Although finite models have extensively proven their ability to describe local properties [21–23], we chose periodic models to perform the calculations in this thesis because of the poor convergence of adsorption energies with respect to cluster size and the need to use a considerably large cluster in order to avoid undesirable edge effects.

The slab model is based on the band-structure theory. A bi-dimensional slab is formed by periodically repeating the geometry of the system on the x and y axes. In the third direction (z axes), the periodicity is broken to create the surface. Depending on the basis set used in the periodic calculation, this slab is further repeated in the direction perpendicular to the surface with a large vacuum width between the repeated slabs (see **Figure 2.1**). This periodic approach avoids problems related to the artificial cluster boundaries, once the limitations associated with the model's finite number of layers are under control. Another advantage of supercell models is that they are well suited to studying the influence of the adsorbates coverage on the surface. However, to study low coverage situations with slab models we need to use large supercells, with a concomitant increase in computational costs.
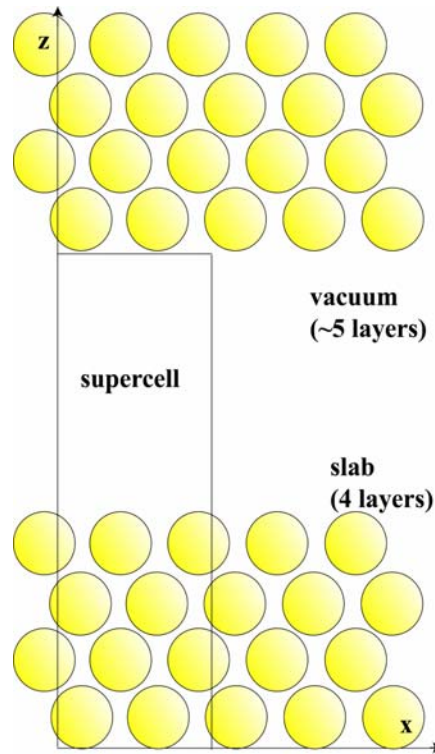
Figure 2.1. Sketch of the slab model. For sake of simplicity, only x and z directions are shown.

2.3.2 Bloch's theorem and the plane wave basis set

In a perfect metallic crystal, atoms are arranged in a regular way. The repeated units of the system are all identical and can be obtained by simple repetition of the unit cell [24]. This means that the Hamiltonian $\hat{H}$ has to commute with the translation operator $\hat{T}$

$$\left[\hat{H},\hat{T}\right]=0 \tag{2.21}$$

Bloch's theorem [25] uses the periodicity of the crystal to reduce the infinite number of the one-electron wave function s to be computed to the number of electrons in the unit cell of the crystal. Then we can express the one-electron wave function s as the product of a cell periodic part and a wave-like part (*Bloch functions*)

$$\psi_{n,\vec{k}}(\vec{R}) = \exp i(\vec{k}\cdot\vec{R})\phi_{nBAND,\vec{k}}(\vec{R}) \tag{2.22a}$$

where $\psi_{n,\vec{k}}$ is the wave function of the periodic system, $\vec{R}$ is the position in the crystal, $\vec{k}$ is a vector of the reciprocal space of the crystal and $\phi_{nBAND,\vec{k}}(\vec{R})$ is a periodic function associated with a band n_{BAND} (or 'energy level' for periodic systems), which has the same periodicity of the system. The problem is then transferred from the real to the reciprocal space. The infinite number of electrons is now mapped onto the problem of expressing the wave function in terms of an infinite number of reciprocal space vectors within the first Brillouin zone [26], $\vec{k}$. Unfortunately, we cannot deal with an infinite number of $\vec{k}$. We can solve this problem by sampling the Brillouin zone at special sets of k-points. The k-points sample can be calculated by various methods. The most popular ones are the Monkhorst-Pack method [27] and the Chadi-Cohen [28] method.

The total wave function at each k-point can be expressed in terms of a discrete plane-wave basis set (3D-Fourrier series)

$$\psi_{n,\vec{k}}(\vec{R}) = \sum_{\vec{g}} a_{nBAND,\vec{g},\vec{k}} \exp i(\vec{g}+\vec{k})\vec{R} \tag{2.22}$$

In principle this set is infinite but we can consider it converged for large values of $\left|\vec{g}+\vec{k}\right|$. Introducing a plane-wave energy cut-off $\left|\vec{g}+\vec{k}\right| < G_{cut-off}$ reduces the basis set to a finite size. This energy cut-off value depends on the system one is working with. Therefore, it is strictly necessary to test the convergence of the energy for a given cut-off value. Moreover, the use of plane-waves forces us to describe the vacuum with the same accuracy as the regions of high electronic density (atoms). Usually a large number of plane waves are necessary.

Using pseudopotentials reduces the $E_{cut-off}$ and, consequently, the size of the expansion.

2.4 Using Pseudopotentials. The PAW method

Working with transition metals involves dealing with a large number of electrons, so the computational time increases exponentially as the system size increases. 'Luckily', the chemical bond does not strongly depend on the core electrons. In fact, only the bonding energy is affected by the average electrostatic potential generated in the vicinity of the core. The aim is then to model the core electrons and their interaction with the other electrons.

The concept of *pseudopotential* dates from the 1930s, when Fermi and Hellmann proposed solving the Schrödinger equation for the valence electrons in the subspace orthogonal to the core electrons. This concept was extended and led to the development of

pseudopotential methods such as 'norm-conserving' pseudopotentials [29], ultra-soft pseudopotentials (US-PP) [30] and the Projector Augmented Wave (PAW) method [31].

The PAW method, introduced by Blöchl, is built on projector functions that allow the complicated wave functions to be mapped onto 'pseudo' wave functions, which are easier to treat computationally. With this method, we model the core electrons taking the difference between the 'true' wave function and a pseudo-wave function obtained and neglecting the core electrons. The Schrödinger equation is then expressed as

$$\tau^* H \tau \tilde{\Psi} = E \tau^* \tau \tilde{\Psi} \tag{2.23}$$

where $\tilde{\Psi}$ is the pseudo wave function and τ is the operator of transformation that connects the exact wave function (Ψ) and the pseudo-wave function ($\tilde{\Psi}$).

In DFT, we solve the Schrödinger equation to determine the 'pseudo'-wave functions. Projectors then enable us to obtain the exact density (whenever the basis set expansion is complete).

The PAW method has extensively proven its high performance for studying molecules, surfaces and solids. We therefore used these pseudopotentials to perform our calculations.

2.5 The VASP code

The program VASP (Vienna *Ab initio* Simulation Package), developed by G. Kresse, J. Furthmüller and J. Hafner [32], has been used for all the calculations in this thesis. This code applies DFT to periodical systems, using plane waves and pseudopotentials. VASP includes an optimised set of US-PP and PAW potentials for all elements of the periodic system.

In VASP, the Kohn-Sham equations are solved self-consistently with an iterative matrix diagonalisation combined with the Broyden/Pulay mixing method [33,34] for charge density. Combining these two techniques makes the code very efficient, especially for transition metal systems that present a complex band structure around the Fermi level. The algorithms implemented in VASP are based on the conjugate gradient scheme, the block Davidson scheme or a residual minimisation scheme (RMM). These algorithms work as follows: they calculate the electronic ground state for a given geometry, calculate forces, and then, based on these forces, predict a new geometry. These steps are then repeated until an energy convergence criterion is reached. A special algorithm is the *quasi*-Newton, where the energy criterion is ignored and only the forces are minimised. A detailed description of the algorithms implemented in VASP can be found in references [35,36].

The Hamiltonian is determined in pieces in direct and reciprocal space. Fast Fourrier Transformations (FFT) are used to switch from direct to reciprocal space and *vice-versa*. This allows for partial diagonalisation.

Besides the pure local density approximation LDA, several gradient-corrected functionals are implemented in VASP to account for the non-local in the exchange-correlation (BP, PW91, PBE).

The number of k-points in the irreducible part of the Brillouin zone is crucial for accurately integrating the properties computed. The k-points sample is usually calculated by the program using the Monkhorst-Pack method [27]. To improve the convergence with respect the k-points sampling, several techniques can be used: the linear tetrahedron method, smearing methods such as finite temperature approaches or improved functional form (Methfessel and Paxton method [37], and finite methods such as gaussian or fermi smearing).

Transition state structures and energies can also be found by various techniques (NEB, Dimer method) implemented in the VASP code. Frequencies and normal modes can also be calculated with this code. Unfortunately, intensities cannot be directly computed.

Further information about VASP can be found at:
http://cms.mpi.univie.ac.at/vasp/vasp/vasp.html.

2.6 Vibrational analysis

2.6.1   Experimental Techniques

Vibrational data on the adsorbates have been widely used to determine the bonding pattern of the adsorbed species, including what sort of site the adsorbate has adopted. It is also very useful for providing valuable information about any fragmentation or reaction that has taken place. Two main techniques have been developed for studying vibrations of adsorbed species on single-crystal metallic surfaces: high-resolution electron energy loss spectroscopy, HREELS (or vibrational EELS, VEELS) and reflection adsorption infrared spectroscopy, RAIRS. We can find detailed and accurate descriptions of these techniques in references [38–42]. Here we will only sketch the most important points.

2.6.1.1 Reflection Adsorption Infrared Spectroscopy (RAIRS)

The application of IR techniques to surfaces owes much of its early development to the work of Eichens, Sheppard and Greenler. Reflection-adsorption infrared spectroscopy (RAIRS) allows for the study of metallic films, single crystals and opaque solids by reflection. This technique has also proved to be a particularly powerful research tool for studying adsorbed phases on metal surfaces. Greenler [43] was the first to demonstrate that the absorption of IR radiation by adsorbates on metallic films is enhanced at high angles of incidence. **Figure 2.2** illustrates the plane of incidence (which contains the incident and the reflected rays and the surface normal), and the so-called *s* (perpendicular to the plane of incidence) and *p* (parallel to the plane of incidence) components of the radiation. At the interface, the p-polarised radiation has a net amplitude almost twice that of the incident radiation (p+p').On the other hand, for s-polarised radiation the incident and emitted rays (s and s') undergo a 180º transformation with respect to each other, so the net amplitude of the radiation parallel to the surface is zero. As a result, only vibrations with a component of the dynamic dipole that is polarised in the direction normal to the surface can be observed in RAIRS.
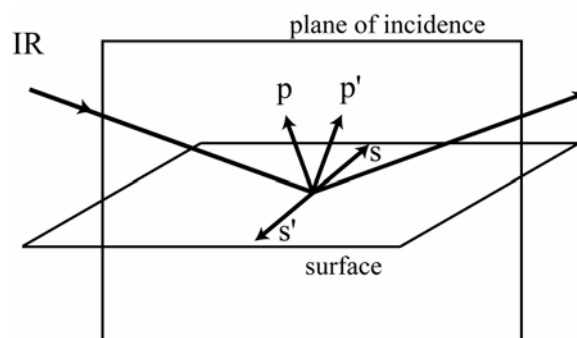
Figure 2.2. Definition of the s and p polarised radiation in the RAIRS experiment.

The IR spectrum of an adsorbate is recorded by tacking a single reflection of an infrared beam at high angles of incidence and taking the ratio of the resulting spectrum to the spectrum obtained for the reflection off the clean surface. The presence of the adsorbate causes small changes in reflectivity at the frequencies of the adsorbate vibrations, where IR radiation is absorbed.

Surface IR spectroscopy can be performed only if the substrate does not absorb strongly. Depending on the substrate, this leads to a cut-off in the 500–1000 cm^{-1} region of the spectrum. The vibrational frequencies of both substrate-adsorbate bond and surface phonons are too low to be studied by this technique.

2.6.1.2 High Resolution Electron Energy Loss Spectroscopy (HREELS)

In the early 1970s, Ibach and co-workers revolutionised surface science thanks to the development of this technique as a surface probe. Early studies demonstrated that HREELS is sensitive to adsorbates with relatively weak dynamic dipoles. At that time, IR methods such as RAIRS restricted its application to molecules with large dynamic dipole moments due to the limitations of equipment and detectors. Moreover, HREELS can interrogate the low-frequency region (100–800 cm^{-1}), where RAIRS cannot be used.

In an EELS experiment, the energetic distribution of electrons back-scattered from a sample bombarded with low energy electrons (E_0, typically in the range of about 8–80 cm^{-1}) is measured and the energy analysis is performed around the primary energy along a given direction with respect to the surface normal (see **Figure 2.3**). The energy E (energy of the scattered electrons) at which a signal occurs is (**equation 2.24**)

$$E = E_0 - h\nu \qquad\qquad (2.24)$$

where E_0 is the energy of the incident electrons, h is the Planck's constant and ν is the frequency of the excited vibration.
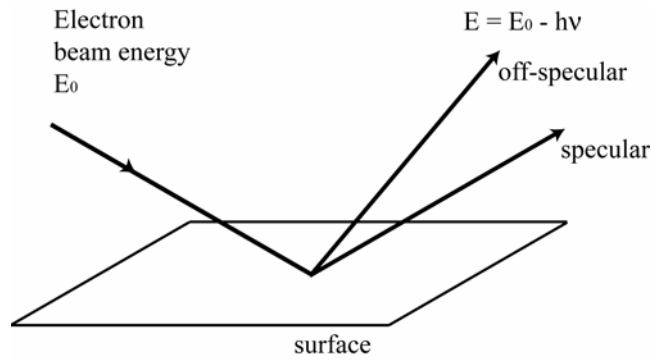
Figure 2.3. Schematic representation of the HREELS experiment.

To correctly interpret EEL spectra we need to know how electrons scatter inelastically. Two types of scattering of electrons can be considered (*dipole* scattering and *impact* scattering). A third mechanism in which an electron is trapped at the surface for a finite time will not be discussed here.

Dipole scattering mechanism

The dipole scattering mechanism is due to the long-range interaction between the electric fields from the incoming electrons and the adsorbate dipoles, which vary in magnitude during the vibration. The scattered electrons are grouped in a small angle around the specular direction. On metal surfaces, the conduction electrons screen the electric field associated with the vibration dipole inside the solid. Therefore, in a first approximation, we need to consider both the electric field generated by the dipole itself and its image underneath the metal surface—the so-called *image-charge* effect. **Figure 2.4** shows that, for an adsorbate dipole of magnitude μ oriented parallel to the surface plane, the image dipole cancels out the surface dipole such that the net dipole is null. However, for a dipole normal to the surface, the presence of the image dipole results in a reinforcement of the net dipole. Therefore, only the vibrating modes that have a component that is perpendicular to the surface are detectable, i.e. only the IR active modes. For this reason, a RAIRS spectrum and a dipolar EELS spectrum are equivalent in terms of band positions, although intensities may vary due to differences in scattering and absorption factors. The absolute intensity of energy loss peaks from the dipole scattering mechanism is expressed as [41,44]

$$\frac{I_{loos}}{I_{elastic}} = \frac{\hbar(1-\theta_E)^{1/2}}{8a_0\varepsilon_0 E_0\cos\theta_I}\left(\frac{\delta\mu}{\delta Q_k}\right)^2\frac{1}{v_k}F\left(\hat{\theta}_c\right)n_s \qquad (2.25)$$
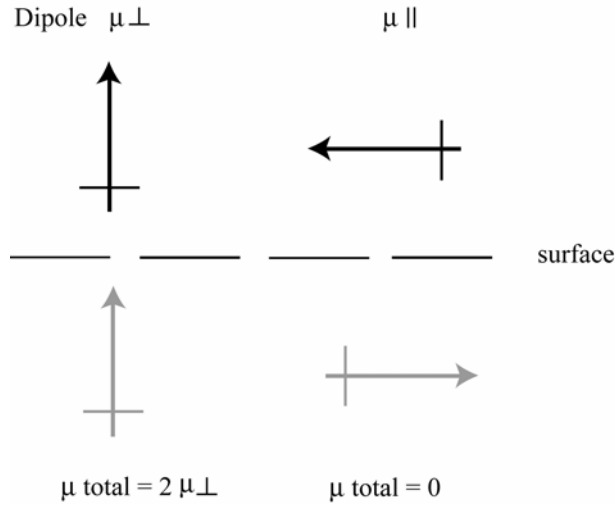
Figure 2.4. Image dipole at a metallic surface.

where a_0 is the Bohr radius, ε_0 is the vacuum permittivity, E_0 is the primary energy of the electron beam, θ_I is the incident angle, $\left(\delta\mu \big/ \delta Q_k \right)$ are the dynamic dipole moment derivatives and n_s [45] is the surface coverage. $F(\hat{\theta}_C)$, θ_E and $\hat{\theta}_C$ are defined as

$$F(\hat{\theta}_C) = \left(\frac{\hat{\theta}_C^2}{1+\hat{\theta}_C^2} (\sin^2(\theta_I) - 2\cos^2(\theta_I) + (1+\cos^2(\theta_I))\ln(1+\hat{\theta}_C^2)) \right) \qquad (2.26)$$

$$\theta_E = \frac{h\nu_k}{2E_0} \qquad \text{and} \qquad \hat{\theta}_C = \frac{\theta_C}{\theta_E} \qquad (2.27 \text{ and } 2.28)$$

where θ_C is the acceptance angle of the spectrometer.

Impact scattering mechanism

This scattering mechanism is best visualised by assuming that the incoming electron 'hits' or 'impacts' the adsorbate and is scattered by the surface atomic potentials, which are modulated at the vibrational frequencies. This mechanism is not subject to the same selection rule as dipole scattering, i.e. the rules valid for RAIRS are no longer appropriate. To determine whether a vibrational mode will lead to an impact scattered loss peak, we need to consider the orientation of the dynamic dipole with respect to the incidence plane of

22

Table 2.1. Comparative physical characteristics of the RAIRS and HREELS techniques

	RAIRS	HREELS
Sample preparation	Easy	Difficult
Temperature range (K)	70-600	Ambient
Pressure range (mbar)	Even above atmospheric P	$\sim 10^{-6}$
Resolution (cm^{-1})	0.5-8	20-80[a]
Lower limit (cm^{-1})	500-1000	<100
Information	Adsorbed species Functional groups	Metal-ligand bonds

[a] advanced spectrometers can now attain 8 cm^{-1}.

the electron beam (specifically to its symmetry elements). This involves group theory, which is beyond the scope of this chapter. In any case, the key point is that it is possible to detect vibrational modes that produce dynamic dipoles both perpendicular and parallel to the metal surface. Impact scattering is only observed in the off-specular direction.

RAIRS and EELS can be considered complementary techniques. **Table 2.1** summarises the main characteristics of these two techniques.

2.6.2 Simulation of vibrational spectra

The theoretical simulation of vibrational spectra is becoming increasingly important in catalysis research. Its uses are diverse. In this thesis we use the theoretically predicted frequencies, intensities and normal modes to corroborate dubious or ambiguous assignments, identify reactive intermediates and characterise transition states.

The vibrational frequencies and the corresponding normal modes were calculated within the harmonic approach using the VASP code. We greatly simplified the vibrational treatment by neglecting the coupling between surface phonons and adsorbate vibrations. We performed several tests to improve the description of the molecule-metal bond vibrations (frequencies below 600 cm^{-1}). To do this we included the two uppermost metal layers in the Hessian matrix. These calculations showed that the frequency changes were always less than 10 cm^{-1} (for more details see **Chapter 3**).

In VASP, the Hessian dynamical matrix is built with finite differences of the first derivatives of the total energy by geometrical perturbation of the optimised Cartesian coordinates. To establish the step length for these numerical differences, we performed extensive tests. These displacements should be taken as large as possible to have meaningful numerical values but small enough to avoid going beyond the harmonic region. We explored the 0.005 to 0.05 Å range and established that the optimal step length (Δr_i) was 0.02 Å. The diagonalisation of the Hessian matrix provides the adsorbate frequencies and the corresponding normal modes Q_k with a matrix of weights P_{ij}.

   To our knowledge, VASP does not compute intensities directly but provides the dynamical dipole moment at each configuration used to construct the Hessian matrix. We calculated the first derivatives of the dynamical dipole moment $\left(\frac{d\mu}{dQ_k} \right)$ to estimate the RAIRS and dipolar HREELS intensities for each normal mode. Note that, in RAIRS and dipolar HREELS, only vibrational modes that lead to an oscillating dipolar moment perpendicular to the surface are active. Consequently, to calculate the intensities we only considered the z-component of the dipole moment, μ_z.

   RAIRS intensities are directly related to the square of the first derivative of μ_z with respect to the normal mode Q_k. We evaluated the RAIRS intensities in the Cartesian coordinate system (Δr_i) following

$$I^k \propto \left(\frac{d\mu_z}{dQ_k} \right)^2 = \left(\sum_{i=1}^{3N} \frac{P_{ki}}{\sqrt{m_i}} \frac{d\mu_z}{d\Delta r_i} \right)^2 \tag{2.29}$$

where μ_z is the z-component of the dipole moment, Δr_i are the Cartesian displacements and $\frac{P_{ki}}{\sqrt{m_i}}$ is the mass weighted coordinate matrix of the normal mode.

   To simulate the dipole HREELS spectra, we computed the absolute intensities I_{loss}^k of the energy losses normalised to the elastic peak intensity $I_{elastic}$ as

$$\frac{I_{loss}^k}{I_{elastic}} = \left(\sum_{i=1}^{3N} \frac{P_{ki}}{\sqrt{m_i}} \frac{d\mu_z}{d\Delta r_i} \right)^2 \frac{F(\omega_k)}{\omega_k} n_s \tag{2.30}$$

where n_s [45] is the surface coverage, ω_k is the calculated frequency associated with a given normal mode and $F(\omega_k)$ is a function of some fixed experimental parameters (energy of the electron beam and working angles; see **equations 2.26** to **2.28**).

$$F(\omega_k) = F(\hat{\theta}_C)(1 - \theta_E)^{1/2} \tag{2.31}$$

2.7 Transition state search

   Precise knowledge of the reaction energetics is essential for determining the minimum energy pathway leading from reactants to the desired products. Also, the possible intermediates and transition states need to be identified. At minima (reactants, products and intermediates) and transition states, the first derivatives of the energy (forces) must be zero.
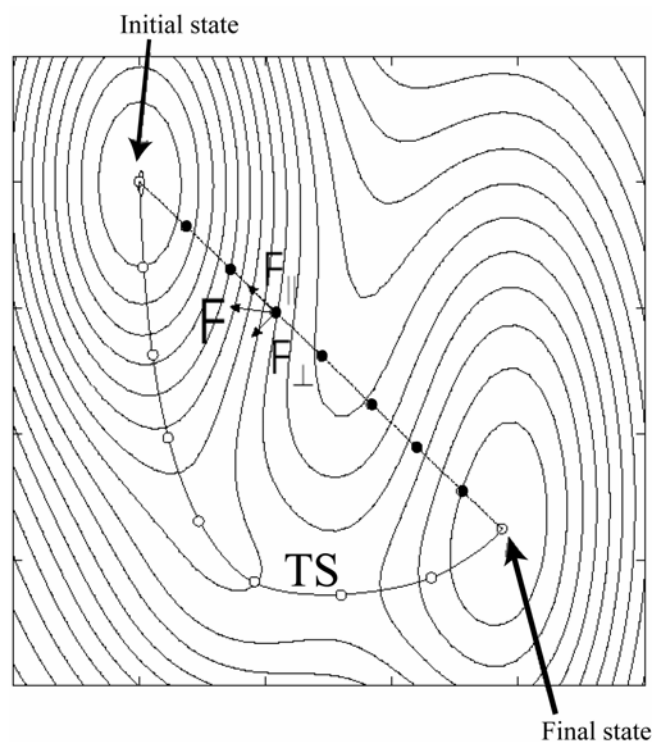
Figure 2.5. Schematic representation of the Nudged Elastic Band method. Starting from an initially guessed reaction path (black dot) the chain settles to the minimum energy path (white dot).

However, unlike minima, transition states (i.e. first order saddle points) must be a maximum along one direction (the one which connects the reactant and the product minima) and minimum in all the other (perpendicular) directions i.e. the second derivative of the energy with respect to the reaction coordinate is negative but in all the other directions it is positive [46].

Transition state localisation is vital for understanding the energetics of a chemical reaction. A reliable method is therefore needed to obtain them. Jónsson and co-workers developed the two transition state search algorithms implemented in VASP and used during this thesis: the *Nudged Elastic Band (NEB) Method* and the *Dimer method.* These methods are summarised in the next sections.

2.7.1 Nudged elastic band method

The *Nudged Elastic Band (NEB) Method* [47] is an example of what is called a 'chain-of states' method. With these methods, several images or states of the system are connected

to trace out a path of some sort. Two points in the configuration space are needed (initial and final states). First, a set of images ($[R_0, R_1, R_2 ... R_N]$, N-1 replicas) between the initial and final states, typically in the order of 4–20, is obtained by linear interpolation (**Figure 2.5**). This is the most important step in the method: the initial guess has to be good enough to converge to a realistic Minimum Energy Path (MEP).

With the NEB method, the N-1 images are optimised with respect to all degrees of freedom except that of the reaction pathway. A spring constant is added to ensure the continuity of the path. The total force on an atom is the sum of the true force perpendicular to the local tangent and the spring force along the local tangent. The projection of the parallel component of the true force acting on the images and the perpendicular component of the spring force are cancelled.

$$F_i = F_i^s\,|_{\parallel} - \nabla E(R_i)\,|_{\perp} \tag{2.32}$$

The two projections are

$$\nabla E(R_i)\,|_{\perp} = \nabla E(R_i) - \nabla E(R_i)\hat{\tau}_i \tag{2.33}$$

and

$$F_i^s = k\left(\left|R_{i+1} - R_i\right| - \left|R_i - R_{i-1}\right|\right)\hat{\tau}_i \tag{2.34}$$

Here, E is the energy of the system, k is the spring constant and τ_i the normalised local tangent at the image i. The above definition of the spring force ensures the constant spacing of the images. The program will run each image simultaneously and communicate the forces at the end of each ionic cycle to compute the force acting on each replica. The minimisation of the forces acting on the images would bring the NEB to MEP.

Usually the number of images in NEB is too small for the length of the path and none of the images lies near to the transition state at the end of the minimisation process. Saddle point energy needs to be estimated by interpolation. The CI-NEB [48] was developed to cope with this problem. After several runs with the 'regular' NEB, the highest energy image is identified (*imax*). This image is treated particularly and the force acting on it is now calculated as

$$F_{i\max} = -\nabla E(R_{i\max})\,| + 2\nabla E(R_{i\max})\,|_{\parallel} \tag{2.35}$$
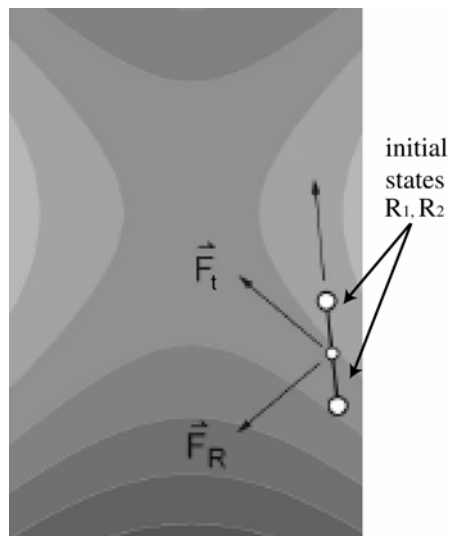
Figure 2.6. Schematic representation of the Dimer method.

where $2\nabla E(R_{i\,max})|_\parallel$ is twice the opposite of the true force parallel to the local tangent. The highest energy image is no longer affected by the spring forces. The minimisation of this force leads to a rigorous convergence to the saddle point.

2.7.2   The Dimer method

The *Dimer method* [49] involves working with two images (replicas, R_1 and R_2) of the target system (n atoms). This pair of images is called 'dimer'. These two replicas have almost the same 3n coordinates, but are displaced a small distance from a common midpoint (centre of the dimer). The saddle point search algorithm involves moving the dimer uphill on the potential energy surface. There are two parts to each move: rotating and translating the dimer. Each time the dimer is translated, it has to be rotated in order to find the lowest curvature mode (lowest energy orientation). A rotational force $\vec{F}_R$ is defined which is the difference in the force on the two replicas. Minimising the energy with respect to this rotational force aligns the dimer with the lowest curvature mode (see **Figure 2.6**).

The saddle point is at a maximum along the lowest curvature direction. As well as being rotated, the dimer has to be translated and moved up the potential energy surface. The net force acting on the centre of the dimer tends to pull it towards a minimum.

To avoid this, an effective force $\vec{F}_t$ on the dimer is defined. In this modified force, the true force due to the potential acting in the midpoint of the dimer is defined as the opposite of the component along the dimer. Minimising with respect to this force brings the dimer to the saddle point.

In this thesis the *Nudged Elastic Band* method was used in combination with the *Dimer* method to determine the transition states. After a few iterations with the NEB, we obtained a rough estimate of the shape of the MEP. We then chose the two images with the highest energy to be the starting point for the Dimer method. Our results were refined until the value of the forces with the *quasi*-Newton algorithm implemented in VASP was negligible. We found that this sequence of algorithms (NEB, *Dimer*, *quasi*-Newton) was the most efficient for the transition state search.

We verified the transition states identified with the NEB and Dimer methods by vibrational frequency analysis (see **section 2.6.2**), yielding a single negative/imaginary frequency. This imaginary frequency has to be consistent with the reaction path under study.

2.8 Density of states

One of the main objectives of computational surface science is to establish a detailed understanding of the adsorption process. *Density of States* (DOS) is an important tool for studying electronic interactions in periodic systems. For each energy E, DOS gives the number of states in the interval [E, E+δE]

$$DOS(E) = \frac{number\ of\ states\ between\ E\ and\ E + \partial E}{\partial E} \tag{2.36}$$

Moreover, we can split the 'total' DOS into the different contributions of the atomic orbitals. In VASP the local orbitals are the spherical harmonics. We define the 'projected' Density of States (PDOS) as the projection of the 'total' DOS onto the spherical harmonics (of fixed radius) of each atom. With this approach, it is easier to analyse the character of the bond.

2.9 Temperature and pressure phase diagrams

DFT is often described as a zero-temperature, zero-pressure technique. To determine the stable phase at a given temperature and pressure, we must compute the Gibbs free energy for all the competing phases. In this thesis, we calculated the temperature pressure diagrams using a simple thermodynamical model [50] in which the gas phase plays the role of a reservoir in equilibrium with the surface and the substrate phase. Thus, it imposes its pressure and temperature on the adsorbed phase. The free Gibbs energy is expressed as:

$$\Delta G(T, P) = \theta \left(E_{ads} + \Delta ZPE - RT \ln\left(\frac{q_{ads}}{q_{gas}}\right) - RT \log\left(\frac{P}{P_0}\right) \right) \tag{2.37}$$

where θ is the surface coverage, E_{ads} is the adsorption energy (calculated with VASP), ΔZPE is the variation of the zero-point energy between the adsorbed phase and the gas-phase plus the clean slab, q_{ads} and q_{gas} are the partition functions of the adsorbed and gas phase, respectively, and the last term comes from the temperature pressure dependence of the gas phase chemical potential.

ΔZPE is small since the hardest molecular frequencies are not significantly affected by the surface process and therefore do not contribute to the free Gibbs energy. Additional approximations were made to evaluate the partition functions. The partition function of the gas phase molecule is expressed as

$$q_{gas} = q_{gas}(rot)q_{gas}(trans)q_{gas}(vib) \tag{2.38}$$

For the adsorbed case the rotational and translational contributions are transformed into additional vibrational contributions

$$q_{ads} = q_{ads}(vib) \tag{2.39}$$

Finally, we assumed that the vibrational partition functions of the gas-phase, the adsorbed system and the clean surface are rather similar so they can be cancelled out; then:

$$\frac{q_{ads}}{q_{gas}} \approx \frac{1}{q_{gas}(rot)q_{gas}(trans)} \tag{2.40}$$

For a given value of temperature and pressure, the favoured coverage is the one that leads to minimum ΔG. However, we should bear in mind that all our approximations were rather crude and the values obtained only provided general trends in adsorption.

2.10 Computational Details

In the previous sections we established the method and model we used to perform all the calculations in this thesis.

To obtain generally uniform results, certain parameters have to be controlled: the DFT lattice constant of the metal (i.e. metal-metal distance), the ideal cut-off of the plane wave expansion, and the number of k-points needed to converge the energy. Also, the vacuum width between adjacent slabs and the thickness (number of layers) of the slabs have to be determined.

First of all, we determined the DFT lattice constant that minimises the energy of the elementary mesh. In this thesis we studied four different metal surfaces: Cu, Pt, Pd and Rh. We optimised the metal-metal interatomic distance for the bulk and obtained the following values: 2.57 Å (Cu–Cu), 2.82 Å (Pt–Pt), 2.80 Å (Pd–Pd) and 2.72 Å (Rh–Rh). All these values are very close to the experimental ones. In fact, the differences are less than 2% [51].

We obtained a tight convergence of the plane-wave expansion with a cut-off of 400 eV. This is the value we used to perform all the calculations in **Chapters 4** and **5**. However, we used a larger value (500 eV) to compute the geometry optimisations and frequency calculations in **Chapter 3**.

For our purposes, we considered several unit cells: √3x√3, 2x2, 3x2, 4x2 4x√3 and 3x3. We performed the 2D Brillouin integrations on a 7x7x1 grid for the √3x√3 unit cells, 5x5x1 for the 2x2 structures, on a 3x5x1 grid for the 3x2 and 4x2, 3x7x1 for the 4x√3 and on a 3x3x1 k-mesh for the 3x3 unit cells. We checked that this density of k points provided a correct convergence of the adsorption energy in the case of the 3x3 unit cell with a difference of ~4 kJmol^{-1} between the 3x3x1 and 5x5x1 grids. Moreover, the energy differences among various adsorption modes were not modified at all when the grid was changed. However, we increased the number of k-points to compute the DOS because these calculations require a denser k-mesh (e.g. for a 2x2 unit cell we used a 7x7x1 k-points grid, for a 3x3 a 5x5x1 mesh …).

We also investigated how the slab thickness and vacuum width affected the adsorption energy.

In agreement with a study of Sautet and co-workers [52], comparison of the four-layer and six-layer slabs showed that the results were consistent only when the k-point convergence was reached and that the six-layer model needed a larger grid. In this thesis the surfaces were modelled by slabs containing four atomic metal layers.

To determine the required vacuum size, we studied the convergence of the adsorption energy using a four layer slab and different vacuum widths. We found that adsorption energies converged for a vacuum width of around 12 Å.

We performed all the calculations on one face of the metal slab (i.e. the target molecule or molecules were adsorbed only on one side of the model). We fully optimised the geometries of the adsorbate and the two uppermost metal planes but kept the two lower metal layers fixed at the optimised bulk geometry.

We computed the adsorption energies (E_{ads}) with the following formula

$$E_{ads} = (E_{C_xH_y/surface} - E_{surface} - E_{C_xH_y(g)}) \tag{2.41}$$

To calculate the relative stabilities of the possible reaction intermediates, we used **equation 4.1** and **5.1** (see **Chapter 4** and **5**).

2.11 References and Notes

[1] M. Born, J.R. Oppenheimer, *Ann. Physik* 84 (1927) 457.

[2] W.J. Here, L. Radom, P.V.R. Schleyer, J. A. Pople, *Ab initio Molecular Orbital Theory*, John Wiley, New York (1986).

[3] J. Almlöf, R. Ahlrichs, *Notes on Hartree-Fock theory and related topics* in *European Summer School in Quantum Chemistry 2003, Book I*, B. O. Roos, P.-O. Widmark Eds., Lund University, Lund (2003) 169.

[4] B.O. Roos, *Multiconfigurational (MC) Self-Consistent (SCF) Theory* in *European Summer School in Quantum Chemistry 2003, Book II*, B. O. Roos, P.-O. Widmark Eds., Lund University, Lund (2003) 285.

[5] P.R. Taylor, *Coupled-Cluster Methods in quantum Chemistry* in *European Summer School in Quantum Chemistry 2003, Book II*, B. O. Roos, P.-O. Widmark Eds., Lund University, Lund (2003) 361.

[6] N.C. Handy, *Density Functional Theory* in *European Summer School in Quantum Chemistry 2003, Book II*, B. O. Roos, P.-O. Widmark, Eds., Lund University, Lund (2003) 503.

[7] J.E. Baerends, O.V. Gritsenko, *J. Phys. Chem. A* 101(1997) 5383.

[8] M. Head-Gordon, *J. Phys. Chem*. 100 (1996) 13213.

[9] L.H. Thomas, *Proc. Camb. Phil. Soc*. 23 (1927) 542; E. Fermi, *Rend. Accad. Lincei*. 6 (1927) 602.

[10] H. Hohenberg, W. Kohn, *Phys. Rev. B* 136 (1964) 864.

[11] W. Kohn, L.J. Sham, *Phys. Rev. A* 140 (1965) 1133.

[12] S. H. Vosko, L. Wilk, M. Nusair, *Can. J. Phys.* 58 (1980) 1200.

[13] A. D. Becke, *J. Chem. Phys.* 84 (1986) 4524; A. D. Becke, *Phys. Rev. A. 38* (1988) 3098; J. P. Perdew, *Phys. Rev. B*. 33 (1986) 8822; J. P. Perdew, *Phys. Rev. B*. 34 (1986) 7406; J. P. Perdew, Y. Wang, *Phys. Rev. B*. 33 (1986) 8800; C. Lee, W. Yang, R. G. Parr, *Phys. Rev. B*. 37 (1988) 785; J.P. Perdew, K. Burke, M. Ernzerhof, *Phys. Rev. Lett*. 77 (1996) 3865.

[14] A. D. Becke, *J. Chem. Phys.* 98 (1993) 5648.

[15] G.Y. Sun, J. Kurti, P. Rajczy, M. Kertesz, J. Hafner, G. Kresse, *J. Molec. Struc. Theochem* 624 (2003) 37.

[16] G. Pacchioni, *Heterogeneous Chemistry Reviews* 2 (1996) 213.

[17] F. Illas, J.M. Ricart, *Química cuántica en materia condensada: aplicación al estudio de superficies, quimisorción, catálisis heterogénea y propiedades de sólidos* in *Química teórica y computacional*, J. Andrés and J. Beltran Eds., Universitat Jaume I, Castelló de la plana (2001) 217.

[18] J. Sauer, *Chem. Rev*. 89 (1989) 199.

[19] G.Pacchioni, P.S. Bagus, F. Parmigiani (Eds.), *Cluster Models for Surface and Bulk Phenomena,* NATO ASI Series B, Volume 283, Plenum Press, New York, 1992.

[20] N.W. Ashcroft, I. Mermin, N. David, *Solid State Physics*, W.B. Saunders Company, New York (1976).

[21] D. Curulla, A. Clotet, J.M. Ricart, F. Illas, *J. Phys. Chem*. 103 (1999) 5246.

[22] D. Curulla, R. Linke, A. Clotet, J.M. Ricart, J.W. Niemantsverdriet, *Phys. Chem. Chem. Phys.* 4 (2002) 5372.

[23] A. Gil, A. Clotet, J.M. Ricart, G. Kresse, M. Garcia-Hernandez, N. Rösch, P. Sautet, *Surf. Sci.* 530 (2003) 71.

[24] The unit cell of a system is not unique. We can choose the unit cell with the smallest volume, the one with the better symmetry properties or the Wigner-seitz unit cell.

[25] C. Cohen-Tannoudji, B. Diu, F. Lalöe, *Mechanique quantique*, Hermann, Paris (1994).

[26] Wigner-Seitz unit cell but in the reciprocal lattice.

[27] H.J. Monkhorst, J.D. Pack, *Phys. Rev. B* 13 (1976) 5188.

[28] D.L. Chadi, M.L. Cohen. *Phys. Rev. B* 59 (1999) 1758.

[29] D.R. Hamann, M. Schlüter, C. Chiang, *Phys. Rev. Lett*. 43 (1979) 1494; G.B. Bachelet, M. Schlüter, C. Chiang, *Phys. Rev B* 26 (1982) 4199.

[30] D. Vanderbilt, *Phys. Rev B* 41 (1990) 7892.

[31] P. Blöchl, *Phys. Rev. B* 50 (1994) 17953.

[32] G. Kresse, J. Hafner, *Phys. Rev. B* 47 (1993) 558; G. Kresse, J. Hafner, *Phys. Rev. B* 48 (1993) 13115; G. Kresse, J. Hafner, *Phys. Rev. B* 49 (1994) 14251; G. Kresse, J. Furthmüller, *Comp. Mat. Sci.* 6 (1996) 15; G. Kresse, J. Furthmüller, *Phys. Rev. B* 54 (1996) 11169.

[33] D.D. Johnson, *Phys. Rev.* B 38 (1988) 12087.

[34] P.Pulay, *Chem. Phys. Lett.* 73 (1980) 393.

[35] G. Kresse, J. Furthmüller, *Comput. Mat. Sci.* 6 (1996) 15.

[36] G. Kresse, J. Furthmüller, *Phys. Rev. B* 54 (1996) 11169.

[37] M. Methfessel, A.T. Paxton, *Phys. Rev. B* 40 (1989) 3616.

[38] M.E. Pemble, *Vibrational Spectroscopy from Surfaces* in *Surface analysis- The Principal Techniques*, Edited by J. C. Vickerman, John Wiley and Sons Ltd., New York(1997) 267.

[39] E.M. McCash, *Surface Chemistry*, Oxford University Press, Oxford (2001)

[40] G. Coudurier, F. Lefebvre, *Infrared Spectroscopy* in *Catalyst Characterisation, Physical Techniques for Solid Materials*, Edited by B. Imelik and J.C. Vedrine, Plenum Press, New York(1994) 11.

[41] J.C. Bertolini, *Vibrational Electron Energy Loss Spectroscopy* in *Catalyst Characterisation, Physical Techniques for Solid Materials*, Edited by B. Imelik and J.C. Vedrine, Plenum Press, New York(1994) 271.

[42] K.W. Kolanski, *Surface Science, Foundations of Catalysis and Nanoscience*, John Wiley and Sons Ltd., West Sussex (2002).

[43] R.G. Greenler, *J. Chem. Phys.* 44 (1966) 310.

[44] Y. Morikawa, *Phys. Rev. B* 63 (2001) 033405.

[45] Coverage is usually represented by the symbol θ. Not used here to avoid any misunderstanding.

[46] J.W. McIver, A. Komornicki, *J. Am. Chem.. Soc.* 94 (1972) 2625.

[47] H. Jónsson, G. Mills, K. W. Jacobsen, Nudged elastic band method for finding minimum energy path of transitions, Classical and Quantum Dynamics in condensed Phase Simulations, J. B. Berne, G. Ciccotti, D. F. Coker Eds, World Scientific, Singapore, 1998, 385.

[48] G. Henkelman, B. P. Uberuaga, H. Jónsson, *J. Chem. Phys*. 113 (2000) 9901.

[49] G. Henkelman, H. Jónsson, *J. Chem. Phys*. 111 (1999) 7010.

[50] K. Reuter, M. Scheffler, *Phys. Rev. B* 65 (2001) 035406.

[51] the experimental values are 2.55 Å, 2.77 Å, 2.75 Å and 2.69 Å for Cu, Pt, Pd and Rh, respectively. R.W.G. Wyckoff, in: *Crystal Structures*, 2nd ed., vol. 1, Interscience, New York (1965).

[52] C. Morin, D. Simon, P. Sautet, *J. Phys. Chem. B* 107 (2003) 2995.